Band Structures of Bilayer Graphene Superlattices

Matthew Killi,[1] Si Wu,[1] and Arun Paramekanti[1,2,3]

[1]*Department of Physics, University of Toronto, Toronto, Ontario, Canada M5S 1A7*
[2]*Canadian Institute for Advanced Research, Toronto, Ontario, M5G 1Z8, Canada*
[3]*Department of Physics, Indian Institute of Science, Bangalore, India 560 012*

We formulate a low energy effective Hamiltonian to study superlattices in bilayer graphene (BLG) using a minimal model which supports quadratic band touching points. We show that a one dimensional (1D) periodic modulation of the chemical potential or the electric field perpendicular to the layers leads to the generation of zero-energy anisotropic massless Dirac fermions and finite energy Dirac points with tunable velocities. The electric field superlattice maps onto a coupled chain model comprised of "topological" edge modes. 2D superlattice modulations are shown to lead to gaps on the mini-Brillouin zone boundary but do not, for certain symmetries, gap out the quadratic band touching point. Such potential variations, induced by impurities and rippling in biased BLG, could lead to subgap modes which are argued to be relevant to understanding transport measurements.

Superlattices provide a route to band structure engineering in semiconductors [1]. In graphene [2], a superlattice (SL) potential has been shown to lead to anisotropic Fermi velocity renormalization [3], and generation of new Dirac points in the spectrum [4–7] resulting from the chiral nature of massless Dirac excitations. Such graphene SLs have been studied by epitaxial growth of graphene on a Ir(111) surface [8,9]. Superlattice effects have also been studied in a topological insulator in proximity to a helical spin density wave [10], and in graphene subject to a magnetic SL [11,12]. However, apart from transfer matrix studies of 1D Krönig-Penney models [7,13], SLs in bilayer graphene (BLG) have not been carefully explored.

Besides band structure engineering, there is a second motivation to study such BLG SLs. On theoretical grounds, BLG is an attractive candidate for transistor applications since it has a tunable gap which varies in proportion to the electric field perpendicular to the layers [14,15]. However, transport measurements on BLG samples do not show strong suppression of conductance at low temperatures expected on theoretical grounds [14,15] or from optical absorption measurements [16]. Instead, the transport data shows evidence for variable range hopping conduction [17–19] or a suppressed band gap [18,20]. It has been proposed that the observed excess conductance arises from edge states [21], but transport measurements in a Corbino geometry do not support this scenario [22], suggesting the existence of disorder-induced low energy modes in the *bulk*. To the extent that disorder potentials can be decomposed into Fourier components, we expect to learn something useful about disordered BLG by studying the simpler problem of periodic potential modulations in BLG.

In this Letter, we study the band structures of BLG SLs, arising from periodic modulations of the chemical potential and the bias, using an effective low energy Hamiltonian. Our main results are the following. (i) Although the minimal model of BLG has quadratic band touching points, we find, remarkably, that a weak 1D chemical potential modulation leads to the generation of linearly dispersing massless Dirac fermions with a tunable and anisotropic velocity. These Dirac fermion excitations are robust and rely on the chiral nature of the BLG quasiparticles. Beyond a critical modulation amplitude, these Dirac modes get gapped out. (ii) An electric field SL is shown to support linearly dispersing massless Dirac fermions and finite energy Dirac points which survive even for strong modulations. We provide a picture for these modes within a novel coupled chain model of "topological" edge states. (iii) For 2D SLs, we show that for chemical potential and electric field SLs the quadratic band touching points are protected for symmetric SLs with C_4 or C_6 symmetry. (iv) We compute the density of states for biased BLG with superimposed 1D potential modulations, and find a plethora of subgap modes which we argue are important for understanding transport data. While our results on 1D SLs overlap with work on Krönig-Penney models [13,23], our analysis provides simpler insights, highlights the role of the quasiparticle chirality, and is applied here to more general potential profiles as well as to 2D SLs.

Effective Hamiltonian approach.—The low energy Hamiltonian for Bernal-stacked BLG can be obtained by expanding its minimal tight-binding spectrum near one of the Brillouin zone corners (**K** points) [14]. When the bias (i.e., interlayer potential difference) is not too large, $|\Delta| \ll t_\perp$, we find $\mathcal{H} = \psi^\dagger \hat{H} \psi$ [14], where

$$\hat{H} = -\frac{v_F^2}{t_\perp}\begin{pmatrix} 0 & (\pi^\dagger)^2 \\ \pi^2 & 0 \end{pmatrix} + \begin{pmatrix} V_1(\mathbf{x}) & 0 \\ 0 & V_2(\mathbf{x}) \end{pmatrix}, \quad (1)$$

and $\psi^T = (a_\mathbf{x}, b_\mathbf{x})$, with a (b) being the electron operator on the top (bottom) layer. Here, $\pi = -i\partial_x + \partial_y$, $v_F = \sqrt{3}td/2 \approx 10^6$ m/s is the Fermi velocity, $t \approx 3$ eV is the nearest neighbor hopping integral, $d \approx 2.46$ Å is the distance between neighboring atoms on the same sublattice, $V_{1,2}$ are the potentials on each layer, and $t_\perp \approx 0.15t$ is the interlayer coupling. Unless stated, we set $t = d = 1$. We will ignore intervalley scattering assuming the potentials are varying slowly on the scale of d, so that identical physics is expected around the other valley (at $-\mathbf{K}$). Such an approach has been successfully used to study SLs in monolayer graphene [3,4].

To diagonalize H_{kin}, we Fourier transform and then make a unitary transformation $a_\mathbf{p} = (\alpha_\mathbf{p} + \beta_\mathbf{p})/\sqrt{2}$, $b_\mathbf{p} = e^{2i\theta_\mathbf{p}}(\alpha_\mathbf{p} - \beta_\mathbf{p})/\sqrt{2}$, where $\cos\theta_\mathbf{p} = p_x/p$ and $p = \sqrt{p_x^2 + p_y^2}$. This leads to $H_{\text{kin}} = \sum_\mathbf{p}(\varepsilon_e(\mathbf{p})\beta_\mathbf{p}^\dagger\beta_\mathbf{p} + \varepsilon_h(\mathbf{p})\alpha_\mathbf{p}^\dagger\alpha_\mathbf{p})$. Here $\varepsilon_{e,h}(\mathbf{p}) = \pm p^2/2m^*$ are energies of electron (hole) states, with an effective mass $m^* \equiv t_\perp/(2v_F^2)$. This minimal model supports quadratic band touching points at $\pm\mathbf{K}$.

When $V_{1,2}(\mathbf{x})$ are periodic, we can also Fourier transform the SL potential to obtain $H_{\text{SL}} = \sum_{\mathbf{p},\mathbf{G}}\Psi^\dagger(\mathbf{p})W_{\mathbf{p},\mathbf{G}}\Psi(\mathbf{p} - \mathbf{G})$, where

$$W_{\mathbf{p},\mathbf{G}} = \frac{1}{2}\begin{pmatrix} V_1(\mathbf{G}) + V_2(\mathbf{G})e^{2i\theta} & V_1(\mathbf{G}) - V_2(\mathbf{G})e^{2i\theta} \\ V_1(\mathbf{G}) - V_2(\mathbf{G})e^{2i\theta} & V_1(\mathbf{G}) + V_2(\mathbf{G})e^{2i\theta} \end{pmatrix}, \quad (2)$$

$\Psi^\dagger(\mathbf{p}) = (\alpha_\mathbf{p}^\dagger, \beta_\mathbf{p}^\dagger)$, and $\theta \equiv \theta_{\mathbf{p}-\mathbf{G}} - \theta_\mathbf{p}$ is the angle between momenta $\mathbf{p} - \mathbf{G}$ and $\mathbf{p}$. Our aim is to understand the band structures of SLs described by $H_{\text{kin}} + H_{\text{SL}}$. We will study 1D SLs with period λ along $\hat{y}$, so that the reciprocal lattice vectors, $\{\mathbf{G}\}$, are integer multiples of $\mathbf{Q} = (0, 2\pi/\lambda)$, and the mini-Brillouin zone (MBZ) boundaries are at $p_y = \pm\pi/\lambda$. We will also study 2D SLs.

1D chemical potential superlattice.—Imposing a periodic potential $V_1(x, y) = V_2(x, y) = U(x, y)$ corresponds to a chemical potential modulation. Numerically solving for the band structure of a periodic 1D modulation using the above effective Hamiltonian, we find a pair of zero-energy
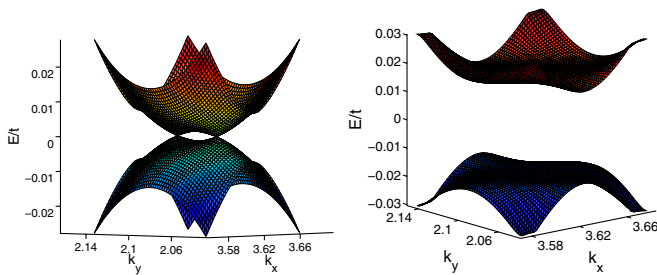
Dirac points in the MBZ in the vicinity of each valley. This is shown in Fig. 1 for a periodic steplike potential with (i) $U(x, y) = U$ for $0 \le y < \lambda/2$ and (ii) $U(x, y) = -U$ for $\lambda/2 \le y < \lambda$. With increasing U, these Dirac points move away from each other along $\hat{y}$. Beyond a critical modulation amplitude a full gap opens up.

The existence of two Dirac cones at each valley is deeply rooted in the chiral nature of the low energy BLG quasiparticles, which causes the matrix elements of Eq. (2) to depend on the scattering angle θ. For states with momenta parallel to the modulation direction, $\theta = 0$ or π, the off-diagonal matrix elements vanish; the electron and hole states then decouple, but electron-electron and hole-hole mixing is allowed. However, in an extended zone scheme, all such electron (hole) states within the first MBZ only mix with electron (hole) states of higher (lower) energy, and so the energy of these states will be globally shifted down (up). This results in two level crossings along the modulation direction, which are protected by the chirality of the low energy BLG quasiparticles. If this electron-hole decoupling was true for all momenta, we would see the two parabolic bands crossing on a full circle in the MBZ, but going to momenta $(\delta p_x, p_y)$ leads to electron-hole mixing that is linear in δp_x; this results in an avoided level crossing and the robust emergence of two Dirac cones in the MBZ.

The location and velocity anisotropy of Dirac cones, as well as the critical modulation amplitude to gap them out, can be predicted using perturbation theory in $U(\mathbf{G})$. The second order energy correction of states with $\mathbf{p} = (0, p_y)$ is $\Delta E^{(2)}(\mathbf{p}) = \sum_{n \ne 0}|U(n\mathbf{Q})|^2/[\varepsilon_{e,h}(\mathbf{p}) - \varepsilon_{e,h}(\mathbf{p} + n\mathbf{Q})]$. Since $\varepsilon_e(\mathbf{p}) < \varepsilon_e(\mathbf{p} + n\mathbf{Q})$ while $\varepsilon_h(\mathbf{p}) > \varepsilon_h(\mathbf{p} + n\mathbf{Q})$ in the MBZ, this correction is always negative (positive) for electron (hole) states, as expected.

Thus, the two bands will intersect and cross linearly at momenta $(0, \pm p_y^*)$, where $p_y^{*2}/2m^* = 2m^*\sum_{n \ne 0}|U(n\mathbf{Q})|^2/(n^2Q^2 + 2p_y^*nQ)$. For weak modulations, $p_y^*/Q \ll 1$, and keeping only $n = \pm 1$, we estimate $p_y^* \approx \sqrt{2}m^*|U(\mathbf{Q})|\lambda/\pi$. For a step profile, $|U(\mathbf{Q})| = 2U/\pi$, and $|n| > 1$ contributions are small.

For small δp_x away from the level crossing point, we can estimate the electron-hole mixing term using perturbation theory [24], and we find that the resulting eigenstates have energies $\epsilon_\mathbf{p} = \pm(16m^*|U(\mathbf{Q})|^2/|\mathbf{Q}|^2)\delta p_x/p_y^*$. The crossing points at $(0, \pm p_y^*)$ are thus really massless Dirac points in the full MBZ. We find velocities $v_y = p_y^*/m^* \approx \sqrt{2}\lambda|U(\mathbf{Q})|/\pi$, and $v_x = 2v_y$ for the anisotropic linear dispersion.

Once these Dirac nodes reach the MBZ boundary, Bragg scattering between them opens up a full gap. The critical potential strength, $|U_c(\mathbf{Q})|$ for this is roughly estimated by setting $p_y^* = Q/2$, which yields $|U_c(\mathbf{Q})| \approx \pi^2/(\sqrt{2}m^*\lambda^2)$. For a step profile, with $\lambda = 60d$, we find $U_c \approx 0.03t$ which is close to the numerical result $0.02t$.

FIG. 1 (color online). Energy spectrum for a 1D superlattice with steplike chemical potential modulation of amplitude U. We set $\lambda = 60d$, with [left panel] $U = 0.01t$ showing two Dirac nodes split along $\hat{y}$ near $\mathbf{K}$, and with [right panel] $U = 0.04t$ showing a full gap.
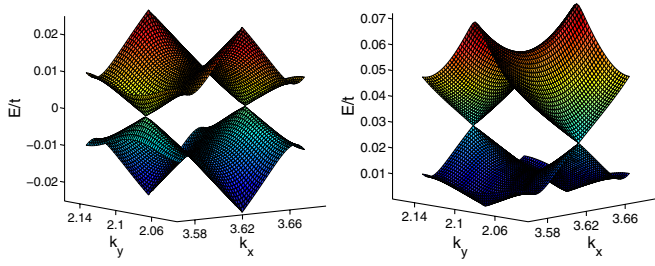
FIG. 2 (color online). Energy spectrum for a 1D symmetric (see text) electric field superlattice with $\lambda = 60d$ and $U = 0.03t$, showing a pair of zero-energy massless Dirac fermions at $(\pm p_x^*, 0)$ [left panel] and a nonzero-energy Dirac point at $(0, \pm \pi/\lambda)$ [right panel].

1D electric field superlattice.—An electric field SL corresponds to $V_1(x, y) = -V_2(x, y) = U(x, y)$. Solving for the resulting band structure, we find that it depends sensitively on the modulation type. To illustrate this, we consider a periodic potential, with $U(y) = 2U(1 - w/\lambda)$ for $0 \le y < w$, and $U(y) = -2Uw/\lambda$ for $w \le y < \lambda$. We have set the average potential on each layer to be zero. If $w = \lambda/2$, the resulting symmetric SL is found to support a pair of anisotropically dispersing massless Dirac fermions at zero energy at $(\pm p_x^*, 0)$, as seen in Fig. 2 (left panel). In addition, as shown in Fig. 2 (right panel), it supports a Dirac point at nonzero positive (as well as negative) energies at $(0, \pi/\lambda)$ [or equivalently $(0, -\pi/\lambda)$]. However, an asymmetric SL, with $w \ne \lambda/2$, leads to a gap for all these Dirac fermions. More generally, we find that if the SL potential commutes with a generalized parity operator, $\mathcal{P}$, which corresponds to $y \to -y$ followed by exchanging the two layers of BLG, then these gapless Dirac points survive. Breaking $\mathcal{P}$ leads to gaps.

A simple route to understanding these results that leads to other interesting predictions is to view the SL as a periodic array of "kinks" and "antikinks" where a kink (antikink) corresponds to where the electric field flips from pointing up (down) to pointing down (up). A single such kink or antikink in the bias is well understood [21,25–27]. In the absence of interactions a kink (antikink) supports a
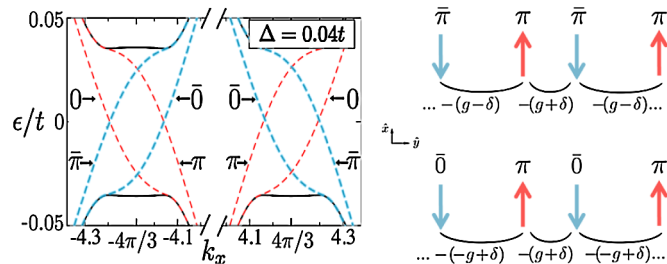
FIG. 3 (color online). Left: Spectrum of isolated kink (thin dashed red line) and antikink (thick dashed blue line). Higher (lower) energy modes are labeled π (0) at a kink and as $\bar{\pi}$ ($\bar{0}$) at an antikink. Right: Schematic of hopping between the $\pi - \bar{\pi}$ and $\bar{0} - \pi$ states.

pair of right-moving (left-moving) "topological" edge states near the $\mathbf{K}$ point for each spin. By time reversal, these right and left movers get interchanged at the $-\mathbf{K}$ point. These modes are depicted in Fig. 3. (Although these modes were suggested to be topologically protected, they are not truly stable against disorder; nevertheless disorder-induced backscattering is weak [21].) At a kink, we denote the higher (lower) energy edge state as π (0), while we denote these states as $\bar{\pi}$ ($\bar{0}$) at an antikink. Hence, there are four points at each valley where kink and antikink modes cross: two of these occur at zero energy ($\pi - \bar{0}$ and $\bar{\pi} - 0$ crossings), and two of them occur at nonzero energy ($\pi - \bar{\pi}$ and $0 - \bar{0}$ crossings). We will show below that these crossing points evolve into massless Dirac fermion modes in the MBZ of the SL. In order to see this, we construct a tight-binding model of such coupled "topological" edge states.

We observe that the Hamiltonian with the single kink (or antikink) potential is invariant under $\mathcal{P}$, since $\mathcal{P}^\dagger H(y)\mathcal{P} = \sigma_x H(-y)\sigma_x = H(y)$. The $0/\bar{0}$ states are even under $\mathcal{P}$, while the $\pi/\bar{\pi}$ states are odd under $\mathcal{P}$ [25]. Let us then construct a reduced Hamiltonian which describes the hybridization between neighboring edge modes.

We begin with neighboring $\pi - \bar{0}$ modes at zero energy and at a momentum p_x^* (away from $\mathbf{K}$). The hopping between neighboring "wires" along $\hat{y}$ is then between states which have opposite velocities (since it is between a kink and an antikink edge state) and it is between a p-wave-like state ($\mathcal{P}$-odd) and an s-wave-like state ($\mathcal{P}$ even). Using the index n to label the wires, the inter-chain hopping parameter will then alternate as $(-1)^n g$ for equally spaced wires and as $g + \delta, -g + \delta$ (with $\delta < g$) if pairs of wires are closer to each other [24]. Linearizing the dispersion at the crossing point, and letting v_0 denote the velocity of the linearized modes,

$$H(p_x) = v_0 \sum_n [(-1)^n (p_x - p_x^*) c_{p_x n}^\dagger c_{p_x n}]$$
$$- \sum_n [g(-1)^n + \delta](c_{p_x n}^\dagger c_{p_x n+1} + \text{H.c.}), \quad (3)$$

where p_x^* is the location of the $\pi - \bar{0}$ crossing point in the single kink or antikink problem, and $c_{p_x n}$ annihilates an electron on wire n with momentum p_x. Let $\xi(p_x) \equiv v_0(p - p_x^*)$. Fourier transforming, we find $H(p_x) = \sum'_{p_y} \Psi^\dagger(p_y) \sigma \cdot \mathbf{h}(p_x) \Psi(p_y)$, where $\mathbf{h}(p_x) = [\xi(p_x), -2g\sin(p_y), -2\delta\cos(p_y)]$, with $\Psi(p_y) = (c_{p_y} c_{p_y+\pi})^T$, and $\sum'_{p_y}$ runs over the MBZ. The dispersion is thus $E = \pm\sqrt{\xi^2(p_x) + 4\delta^2\cos^2(p_y) + 4g^2\sin^2(p_y)}$. Consequently, when $w = \lambda/2$, and the Hamiltonian commutes with $\mathcal{P}$, we have $\delta = 0$ and a Dirac cone is generated at $(p_x^*, 0)$, consistent with numerical results. When $w \ne \lambda/2$, the Hamiltonian breaks $\mathcal{P}$—we then
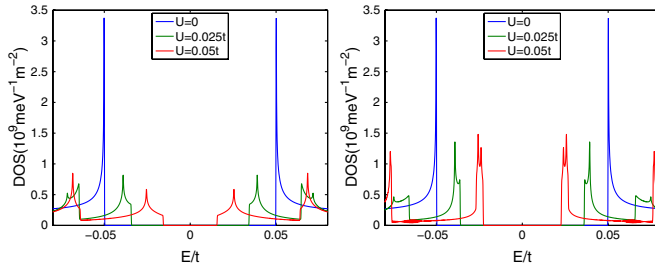
FIG. 4 (color online). Density of states for BLG subject to a uniform bias of $\Delta = 0.1t$ and various chemical potential (left) and electric field (right) superlattices with period $\lambda = 60d$.

have $\delta \neq 0$, which leads to a gap 4δ. Similar arguments hold for the other zero-energy band crossing points. The velocity of the Dirac fermions is highly anisotropic and depends on g—this can be controlled by tuning the SL period and amplitude.

The above analysis can also be repeated for the nonzero energy $(0 - \bar{0}$ and $\pi - \bar{\pi})$ crossings [24]; in the symmetric case, $w = \lambda/2$, we find Dirac cones at $(0, \pm\pi/\lambda)$ on the MBZ. Once again, a modulation with $w \neq \lambda/2$ results in a finite δ and opening of band gap.

Interestingly, just as in polyacetylene, a domain wall between a gapped region with $w > \lambda/2$ and a gapped region with $w < \lambda/2$ leads to new subgap soliton modes. Since each kink or antikink is itself like a domain wall, these should be viewed as solitons in a soliton lattice.

2D superlattices.—We have also considered 2D chessboardlike SLs with fourfold rotation symmetry. For both types of 2D SLs, chemical potential or electric field, the quadratic band touching point remains intact when the SL potential is "symmetric", $V_{1,2}(x + \lambda/2, y) = V_{1,2}(x, y + \lambda/2) = -V_{1,2}(x, y)$. This is consistent with the fact that no Dirac points can be generated in a way that conserves both topological charge and C_4 (or C_6) symmetry [28]. For asymmetric SLs, higher order corrections lead to modifications to the energy spectrum at the **K** point [24]. For chemical potential SLs, the charge neutrality point (CNP) shifts slightly in energy, due to higher order effects which reflect particle-hole symmetry breaking. For electric field SLs, breaking generalized parity opens a small gap at the **K** point [24].

Experimental implications.—Our work demonstrates that SL modulations in BLG can generate new Dirac fermion modes. Such modes are perturbatively stable to interaction effects, and could be experimentally explored by a suitable choice of substrates. Disorder will also lead to such bias and chemical potential modulations, albeit in random fashion. One source of such fluctuations is the presence of charged impurities, embedded in the underlying substrate (SiO_2) or, in the case of suspended BLG, in the residue of the etching or washing process. Such impurities are expected to locally shift the CNP, and to suppress or enhance the band gap depending on the relative sign of the bias and the impurity electric field [29]. If the impurity

lies close to the surface it can locally reverse the parity of the interlayer bias leading to "topological" subgap modes. Another source of SL fluctuations is rippling [30,31], which would modulate the electric field perpendicular to the bilayer at the ripple wavelength.

As a starting point to understanding the expected role of chemical potential and electric field fluctuations, Fig. 4 shows density of states (DOS) plots of a biased SL with periodic 1D modulations. In the absence of a SL, the DOS diverges as $1/\sqrt{E}$ at the gap edge arising from the $\sim p^4$ dispersion of modes near the gap edge. We find that both chemical potential or bias modulations, cause low energy subgap modes in this system that will renormalize the average band gap, consistent with experiments. For chemical potential modulations, the subgap states are due to the local shift in the CNP. At finite temperature, regions with a slightly shifted CNP will have thermally activated "electron-hole" puddles that contribute to transport. For bias modulations, weak modulations locally enhance or suppress the band gap, while strong modulations form "topological" states in the bulk along interfaces where the field reverses sign [21,25–27]. The energy of these "topological" midgap states decreases for large and dilute fluctuations, as the overlap between edge mode wave functions is reduced.

Random potential fluctuations will have two important effects not captured in our study of periodic modulations. First, it will cause the low energy density of states to broaden, causing further suppression of the band gap predicted by the periodic modulation. Second, dilute localized "topological" states induced in the *bulk* by strong random electric field modulations due to charged impurities will contribute to transport through variable range hopping—this is broadly consistent with the temperature dependence of the resistance in biased BLG [17–19].

Note Added.—After submission of this Letter, we received a preprint of Ref. [32], which studies Dirac fermions in 1D chemical potential superlattices in BLG and contains results consistent with ours.

[1] R. Tsu, *Superlattice to Nanoelectronics* (Elsevier, Oxford, UK, 2005).
[2] A. H. Castro Neto *et al.*, Rev. Mod. Phys. **81**, 109 (2009).
[3] C.-H. Park *et al.*, Nature Phys. **4**, 213 (2008).
[4] C.-H. Park *et al.*, Nano Lett. **8**, 2920 (2008); C.-H. Park *et al.*, Phys. Rev. Lett. **101**, 126804 (2008); C.-H. Park *et al.*, Phys. Rev. Lett. **103**, 046808 (2009).
[5] L. Brey and H. A. Fertig, Phys. Rev. Lett. **103**, 046809 (2009).
[6] M. Barbier *et al.*, Phys. Rev. B **77**, 115446 (2008).
[7] M. Barbier *et al.*, Phys. Rev. B **79**, 155402 (2009).
[8] I. Pletikosić *et al.*, Phys. Rev. Lett. **102**, 056808 (2009).

[9] S. Rusponi *et al.*, Phys. Rev. Lett. **105**, 246803 (2010).

[10] Q. Li *et al.*, Phys. Rev. B **83**, 085110 (2011).

[11] L. Dell'Anna and A. De Martino, Phys. Rev. B **83**, 155449 (2011).

[12] M. R. Masir *et al.*, New J. Phys. **11**, 095009 (2009).

[13] M. Barbier, P. Vasilopoulos, and F. M. Peeters, Phys. Rev. B **81**, 075438 (2010).

[14] E. McCann and V. I. Fal'ko, Phys. Rev. Lett. **96**, 086805 (2006).

[15] E. McCann, Phys. Rev. B **74**, 161403(R) (2006).

[16] Y. Zhang *et al.*, Nature (London) **459**, 820 (2009).

[17] J. B. Oostinga *et al.*, Nature Mater. **7**, 151 (2007).

[18] T. Taychatanapat and P. Jarillo-Herrero, Phys. Rev. Lett. **105**, 166601 (2010).

[19] H. Miyazaki *et al.*, Nano Lett. **10**, 3888 (2010).

[20] F. Xia *et al.*, Nano Lett. **10**, 715 (2010).

[21] J. Li, I. Martin, M. Büttiker, A. Morpurgo, Nature Phys. **7**, 38 (2010).

[22] J. Yan and M. S. Fuhrer, Nano Lett. **10**, 4521 (2010).

[23] M. Barbier, P. Vasilopoulos, and F. M. Peeters, Phil. Trans. R. Soc. A **368**, 5499 (2010).

[24] See Supplemental Material at http://link.aps.org/supplemental/10.1103/PhysRevLett.107.086801 for further details.

[25] I. Martin, Ya. M. Blanter, and A. F. Morpurgo, Phys. Rev. Lett. **100**, 036804 (2008).

[26] M. Killi *et al.*, Phys. Rev. Lett. **104**, 216406 (2010).

[27] L. J. P. Xavier *et al.*, Appl. Phys. Lett. **96**, 212108 (2010).

[28] K. Sun *et al.*, Phys. Rev. Lett. **103**, 046811 (2009).

[29] A. Deshpande *et al.*, Appl. Phys. Lett. **95**, 243502 (2009).

[30] M. Ishigami *et al.*, Nano Lett. **7**, 1643 (2007).

[31] W. Bao *et al.*, Nature Nanotech. **4**, 562 (2009).

[32] L. Tan *et al.*, Nano Lett. **11**, 2596 (2011).